RSC Advances

PAPER

View Article Online
View Journal | View Issue

Cite this: *RSC Adv.*, 2018, **8**, 8228

Graphene-supported platinum/nickel phosphide electrocatalyst with improved activity and stability for methanol oxidation†

Jiamu Cao, ‡[a] Hailong Chen,‡[a] Xuelin Zhang,*[ab] Yufeng Zhang[ab] and Xiaowei Liu[ab]

Received 13th December 2017
Accepted 2nd February 2018

DOI: 10.1039/c7ra13303k

rsc.li/rsc-advances

In this paper, we report a novel catalyst using Ni_2P as a cocatalyst of Pt supported on graphene for methanol oxidation. The results reveal that the electrocatalytic activity and stability of the as-prepared catalyst for methanol oxidation are significantly enhanced by the addition of Ni_2P. The reason for the increased activity and stability is ascribed to complex electron transfer between Pt, Ni_2P, and graphene, which gives rise to the eventual promotion of CO_{ads} electrooxidation reaction kinetics. The present study implies that the as-prepared Pt–Ni_2P/graphene will be a promising candidate as an anode electrocatalyst in direct methanol fuel cells.

1 Introduction

The direct methanol fuel cell (DMFC) as a promising power source for portable electronic devices has attracted more and more attention due to its simple system design, high energy density, and low pollutant emission.[1–3] These advantages are enough to make it a promising way to address the existing environmental emission issues from fossil energy.[4] However, reducing cost is an urgent problem to solve in many research fields,[5,6] therefore, reducing the dosage of precious metal catalyst, or improving its catalytic efficiency is an important means to push forward the commercialization of DMFCs.[7]

The main reason for DMFC anode rate limitation is apparently the sluggish electrooxidation of adsorbed carbon monoxide, an intermediate product of anodic methanol oxidation.[8] Efforts to mitigate CO poisoning of Pt nanoparticles can be made through the addition of some metals, such as Ru,[9–11] Sn,[12] Ni.[13] Among them, nickel-based nano-materials not only have been proved to show electrocatalytic activity toward alcohols oxidation but also have been used in the hydrogen evolution reaction,[14,15] the hydrolytic dehydrogenation,[16] the electrolytic hydrogen generation, and the hydrogen peroxide reduction reaction,[17,18] as non-noble metal catalysts.

N-Doped carbon-encapsulated Ni nanoparticles give an effective electrocatalytic activity and long-term stability for ethanol oxidation in the alkaline aqueous electrolyte.[19,20] NiOOH and NiO present the superior methanol electrocatalytic oxidation performance.[21,22] Besides these, Ni_2P was found to be able to enhance the activity and stability of carbon black-supported palladium and platinum nanoparticles toward alcohols,[23–25] which revealed that the incorporation of Ni_2P gives rise to promote the electrooxidation of methanol and resistance to CO poisoning.

On the other hand, the carrier plays an important role in the catalytic performance.[26,27] Graphene, mother of all graphitic forms, is considered as the most promising supporting material for carbon black and carbon nanotube.[28–30] Many metallic compounds which combined with graphene have been reported to form complex hybrid structure and display superior catalytic performance compared to naked particles.[31,32] Graphene sheets in the above structure act as not only a buffer zone of volume change of the active materials but also a good electron transfer medium.[33]

Inspired by these previous findings, we attempt to using graphene as a carrier to examine the possible promotion of Pt by Ni_2P in methanol oxidation for DMFC. To date, we have not found reported findings combining Pt, Ni_2P, and graphene to synthesize high qualified catalyst for methanol oxidation. Herein, we first prepared Pt–Ni_2P/graphene catalyst for DMFC by a microwave assisted ethylene glycol method. The physical structure and electrochemical performance of the as-prepared catalysts were characterized and analyzed. A possible mechanism of the interaction between Pt, Ni_2P, and graphene was also discussed.

2 Experimental

2.1 Synthesis process

The Pt–Ni_2P/graphene catalyst synthesis process as schematically displayed in Fig. 1a. Ni_2P nanoparticles supported on

[a]*Key Laboratory of Micro-Systems and Micro-structures Manufacturing, Ministry of Education, Harbin 150001, China. E-mail: zhangxuelin@hit.edu.cn*

[b]*MEMS Center, Harbin Institute of Technology, Harbin 150001, China*

† Electronic supplementary information (ESI) available. See DOI: 10.1039/c7ra13303k

‡ These authors contributed equally to this work.

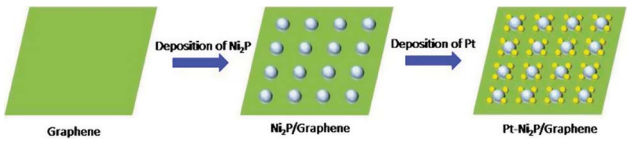

Fig. 1 Schematic diagram of synthesizing Pt–Ni2P/graphene catalyst.

graphene (Ni_2P/G) were first prepared by a typical thermal reaction.[25] The 5 mg GO and 0.3 g NiS_2 were mixed in 20 mL distilled water and subjected to ultrasonic vibration to form a homogeneous suspension. Then 1.03 g $NaH_2PO_2 \cdot H_2O$ was dispersed in 20 mL distilled water and mixed with the above suspension. Then the mixture was calcined at 500 °C for 1 h and cooled to room temperature. The solid obtained was washed thoroughly with distilled water and absolute ethyl alcohol to remove the by-products. After that, the wet products were dried at 80 °C for 12 h in a vacuum oven.

Then the obtained product dispersed into ethylene glycol (EG) and isopropyl alcohol in a breaker under stirring for 1 h and ultrasonic treatment for 3 h to form a uniform ink. Then H_2PtCl_6–EG solution was added and stirred for 2 h. The pH value of the ink was adjusted by NaOH–EG solution drop by drop until its value reached 12. The next step was to place the breaker the center of a microwave oven for consecutive heating time for 65 s. The solution was cooled down to room temperature and then dilute HNO_3 solution was added to the mixture to adjust pH value to 4. The mixture was kept stirring for 12 h and then the product was washed repeatedly with ultrapure water until no Cl^- was detected. The homemade Pt–Ni_2P/graphene catalyst was dried for 3 h at 80 °C in a vacuum oven and then stored in a vacuum vessel. Theoretically, the Pt and Ni_2P loading of the Pt/Ni_2P–graphene was 20 wt% and 5 wt%, respectively. For the purpose of comparison, the Pt/graphene catalyst was prepared without the addition of Ni_2P using the similar procedure mentioned above.

2.2 Preparation of the working electrode

The catalyst slurry was prepared by ultrasonically dispersing 4 mg catalyst in the solution of 0.2 mL ethanol, 0.8 mL ultrapure water and 20 μL Nafion (5 wt% solution in a mixture of lower aliphatic alcohols and DuPont water) for 30 min. A glassy carbon electrode (GCE) with the diameter of 4 mm was polished with alumina suspensions and served as the underlying substrate of the working electrode. A quantity of 5 μL of the dispersion was extracted out on the top of the GC followed by drying at room temperature for 4 h.

2.3 Electrochemical measurements

Electrochemical characterizations of the catalysts were carried out in a standard three-electrode cell using a Pt wire counter electrode and a Hg/Hg_2SO_4 reference electrode at room temperature (*ca.* 298 K). In the following, all potentials were given relative to a reversible hydrogen electrode (RHE). Cyclic voltammetry (CV) was conducted at a scan rate of 50 mV s^{-1} with the potential range from 0 V to 1.2 V. To compare the long-term performance of the catalysts for methanol oxidation, chronoamperometry (CA) tests were used in a solution of 0.5 M H_2SO_4 and 0.5 M CH_3OH for 3000 s with the step potential of 0.6 V. All the electrochemical tests were carried out with CHI650D electrochemical working station.

3 Results and discussion

The elemental and phase compositions of the catalysts were characterized by energy dispersive X-ray spectroscopy (EDS) and X-ray diffraction (XRD). As shown in Fig. 2a, elements of Ni, P and Pt are observed in EDS spectra of Pt–Ni_2P/graphene. Elemental mapping images in Fig. 2b shows that Ni, P, and Pt homogeneously distribute on the transparent graphene nanosheet. The formation of Ni_2P phase in the as-prepared catalyst was confirmed by the XRD patterns, as shown in Fig. 2c, where the observed diffraction peaks of Ni_2P can be indexed to a hexagonal phase. Besides this, the diffraction peaks of Pt (1 1 1), Pt (2 2 0), and Pt (3 1 1) are also observed, indicating Pt forms the face-centered cubic (fcc) crystal structure. These results suggest that nanoparticles of Pt and Ni_2P have been successfully synthesized and supported on graphene. Moreover, it should be noteworthy that the C (002) peak near 25° appears in the pattern of Pt/graphene but is absent in the pattern of Pt–Ni_2P/graphene. This big difference reveals that Ni_2P nanoparticles could reduce the stacking of graphene sheets, acting as a kind of spacer to

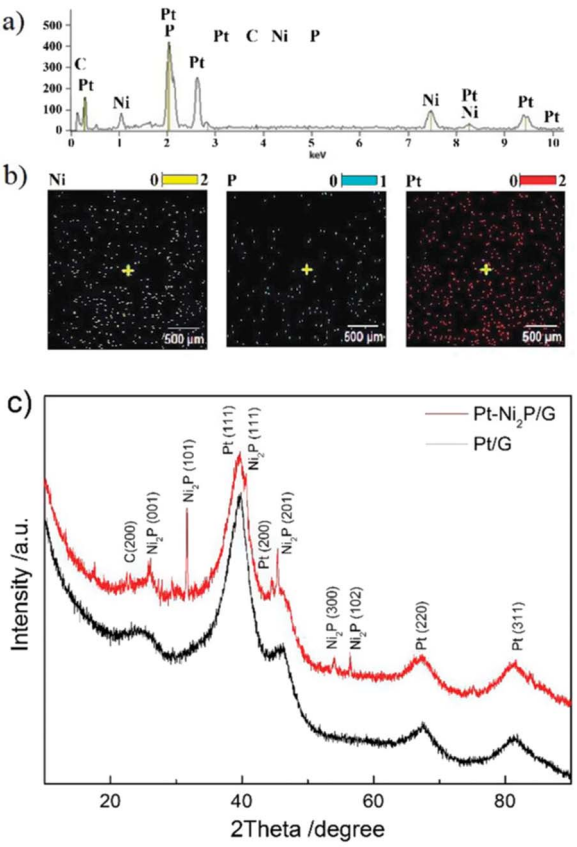

Fig. 2 EDS spectra (a) and elemental mapping images (b) of Pt–Ni_2P/graphene; XRD pattern (c) of Pt–Ni_2P/graphene and Pt/graphene.

help graphene maintain its large surface area and high mass transfer efficiency.

The structure and morphology of the prepared catalysts were characterized by TEM, and the results are shown in Fig. 3a and Fig. 3b. It can be seen that platinum particles are well dispersed on graphene support. The diameters of the Pt particles on the two catalysts range from 2 to 4 nm (Fig. 3d), and the incorporation of Ni_2P does not lead to an obvious change in the sizes of Pt particles. On the HRTEM image (Fig. 3c) describing the crystalline nature of Pt–Ni_2P, Ni_2P nanoparticles can be observed with a finger lattice of 0.502 nm, corresponding to the (111) facet. It also shows the reduced Pt particles have successfully adhered to Ni_2P particles deposited on graphene sheets. In this contact, electron transfer might occur and changes the crystal lattice of atoms, which decrease van der Waals forces between separated graphene sheets, well accounting for the reduced aggregation and disappeared C (002) peak.

To confirm the existence of electron interaction, X-ray photoelectron spectroscopy (XPS) was carried out, and the results are shown in Fig. 4. It can be seen that the Pt 4f peaks of the Pt/G catalyst at binding energies of 69.88 (Pt $4f_{7/2}$) and 72.98 (Pt $4f_{5/2}$) eV move to lower binding energies of 69.08 and 72.28 eV in Pt–Ni_2P/G catalyst, respectively. This shift is likely to an indicator of a partial electron transfer from Ni_2P to Pt, which might change the electronic structure and density of state of Pt atoms and thus weaken the binding energy of strongly adsorbed and poisonous intermediates,[34] laying a theoretical foundation for the enhanced catalytic activity and stability in following electrochemical tests.

In electrochemical tests, the cyclic voltammogram (CV) curves of Pt–Ni_2P/graphene and Pt/graphene were characterized in N_2 saturated 0.5 M H_2SO_4 solution, and the results are shown in Fig. 5a. The electrochemical surface area (ESA) is estimated from the integrated charge in the hydrogen/adsorption region (0.03 to 0.4 V *vs.* RHE) of the CV curves.[35] The ESA of Pt–Ni_2P/graphene is calculated as 86.87 $m^2\ g^{-1}$, 23% higher than that of Pt/graphene (70.32 $m^2\ g^{-1}$), and these values are larger than the previously reported results,[25] indicating that graphene may be able to provide better support for Pt nanoparticles than carbon-black. Moreover, the peak potential of the Pt–Ni_2P/graphene catalyst shifts towards

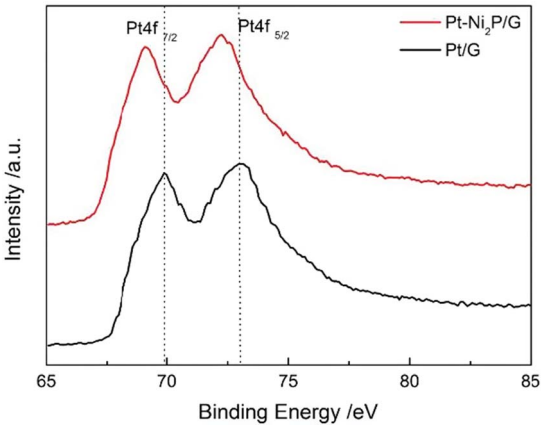

Fig. 4 XPS spectra of Pt 4f region of Pt–Ni_2P/graphene and Pt/graphene catalysts.

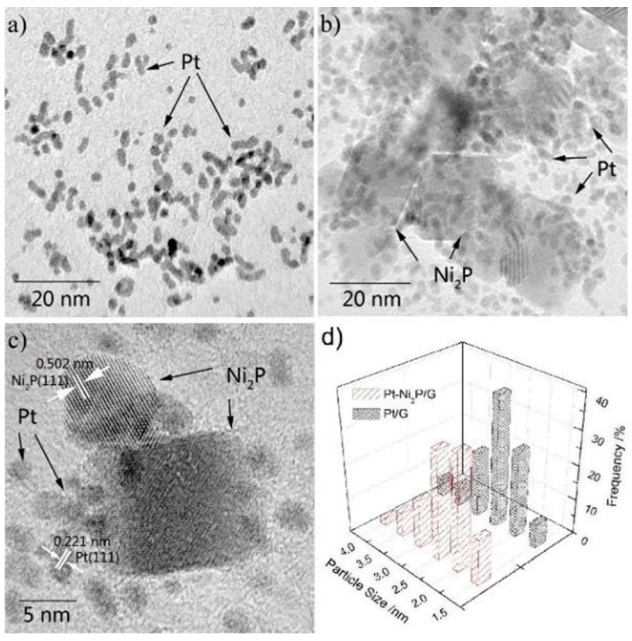

Fig. 3 TEM images of Pt/graphene (a) and Pt–Ni_2P/graphene (b); HRTEM image of Pt–Ni_2P/graphene (c); particle size distribution (d) of Pt–Ni_2P/graphene and Pt/graphene.

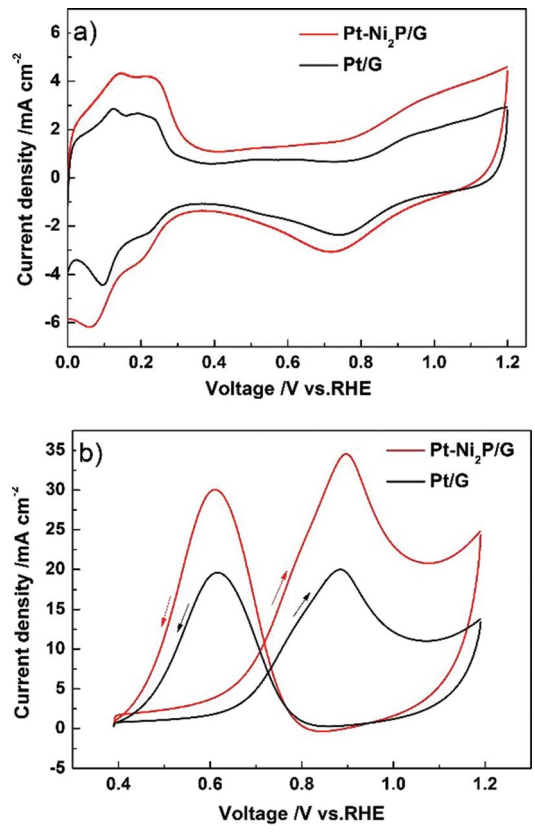

Fig. 5 Cyclic voltammetric curves with a scan rate of 50 mV s^{-1} for Pt–Ni_2P/graphene and Pt/graphene catalysts in N_2 saturated 0.5 M H_2SO_4 (a) and 1 M CH_3OH + 0.5 M H_2SO_4 (b) solutions.

a negative direction when compared to that of the Pt/graphene catalyst, indicating the weakened adsorption strength of hydrogen on the Pt surface.[36] This might be attributed to the hydrogen spillover effect of Ni_2P, which is considered to be beneficial for increasing the electrochemical surface area and eventually enhancing the utilization of Pt catalyst. Furthermore, additional experiments showed that compared with Pt–Ni_2P/graphene, the Ni_2P has almost no catalytic activity (Fig. S1†). The results further illustrated that introducing Ni_2P as cocatalyst can enhance the catalytic activity of the Pt–Ni_2P/graphene due to changing the electronic structure and density of state of Pt atoms and thus weaken the binding energy of strongly adsorbed.

The CV tests in N_2 saturated 0.5 M CH_3OH + 0.5 M H_2SO_4 solution were also conducted to examine the catalytic ability toward methanol oxidation, and the results are shown in Fig. 5b. It can be seen that the Pt–Ni_2P/graphene catalyst exhibits a higher peak current density than Pt/graphene does. The ratio between peak current densities in the forward (i_f) and backward (i_b) scan for Pt–Ni_2P/graphene and Pt/graphene is valued as 1.15 and 1.02 respectively, which reflects that Pt–Ni_2P/graphene has better tolerance to carbonaceous species.[37] This result was further confirmed by the CO stripping test, as shown in Fig. 6. Compared to the Pt/graphene catalyst, the onset potential for CO_{ads} oxidation on Pt–Ni_2P/graphene catalyst is shifted negatively. ESA was also calculated from the CO oxidation area with an assumption that the charge of CO monolayer adsorption is 484 μC cm^{-2}, and the values for the Pt–Ni_2P/graphene and Pt/graphene catalysts are 80.7 $m^2\ g^{-1}$ and 65.9 $m^2\ g^{-1}$, respectively. This result proves that higher MOR activity and tolerance can be achieved with the corporation of Ni_2P cocatalyst in Pt nanoparticles. The reason may be that the addition of Ni_2P can weaken the accumulation of CO-like intermediates at Pt active sites. Moreover, as an initial hydrogen evolution catalyst, the presence of Ni_2P self might also active water and accelerate hydrogen adsorption, producing $-OH_{ads}$ to oxidize CO and other poisoning intermediates adsorbed at adjacent Pt sites through the so-called bifunctional mechanism.[38]

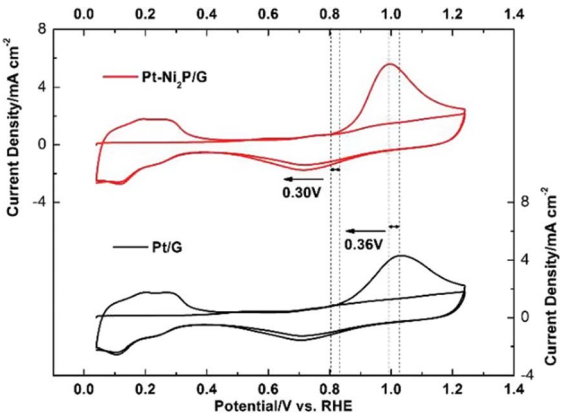

Fig. 6 Cyclic voltammetric curves with a scan rate of 50 mV s^{-1} for Pt–Ni_2P/graphene and Pt/graphene catalysts in CO_{ads} stripping voltammograms.

Finally, the typical current density-time responses at a fixed potential of 0.6 V *vs.* RHE were measured in N_2 saturated 0.5 M CH_3OH + 0.5 M H_2SO_4 solution to test the stability toward methanol oxidation, and the results are shown in Fig. S2.† Because of the formation of intermediate species, such as CO_{ads}, CHO_{ads} during the methanol oxidation reaction,[39] the current densities decrease rapidly with the increment of time from the initial values of *ca.* 4.80 and 3.67 mA cm^{-2} at Pt–Ni_2P/graphene and Pt/graphene, respectively. But, the decay rate at the Pt–Ni_2P/graphene catalyst is obviously smaller than that at the Pt/graphene catalyst. Moreover, after 3000 s, the stable current density at the Pt–Ni_2P/graphene catalyst (*ca.* 1.35 mA cm^{-2}) is evidently higher than that at the Pt/graphene catalyst (*ca.* 0.77 mA cm^{-2}). The result illustrates that the catalyst containing Ni_2P displays favorable stability and higher catalytic activity for methanol oxidation, in agreement with the above results. Furthermore, the TEM images depicted in Fig. S3† showed that the original morphology of the Pt–Ni_2P/graphene catalyst was well preserved after typical current density-time responses measurement.

4 Conclusions

In summary, the Pt–Ni_2P/graphene catalyst was successfully synthesized *via* a microwave-assisted glycol process. The physical and chemical tests reveal that the addition of Ni_2P greatly improves the electrocatalytic activity and stability with respect to methanol oxidation, which is probably attributed to the synergetic effects of an interface between the platinum and Ni_2P and of a spillover due to diffusion of the reaction intermediates. Ni_2P as a cocatalyst of Pt appears to be a promising application for less expensive direct methanol fuel cell.

Conflicts of interest

There are no conflicts to declare.

Acknowledgements

This work was supported by the National Natural Science Funds of China (No. 61404037, 61376113).

References

1 A. A. Kulikovsky, *Electrochem. Commun.*, 2012, **24**, 65–68.
2 Y. Li, X. L. Zhang, L. Nie, Y. F. Zhang and X. W. Liu, *J. Power Sources*, 2014, **245**, 520–528.
3 Z. Yuan, Y. Zhang, W. Fu, Z. Li and X. Liu, *Energy*, 2013, **51**, 462–467.
4 J. M. Cao, J. Zhou, Y. F. Zhang and X. W. Liu, *RSC Adv.*, 2017, **7**, 25867–25871.
5 Y. W. Huang, Q. J. Yu, J. Z. Wang, J. N. Wang, C. L. Yu, J. T. Abdalla, Z. Zeng, S. J. Jiao, D. B. Wang and S. Y. Gao, *ACS Sustainable Chem. Eng.*, 2018, **6**, 438–446.
6 S. M. Ni, Q. J. Yu, Y. W. Huang, J. N. Wang, L. Li, C. l. Yu, F. Y. Guo, H. G. Wu, W. J. Lu and X. T. Zhang, *RSC Adv.*, 2016, **6**, 85951–85957.

7 Y. Vlamidis, S. Fiorilli, M. Giorgetti, I. Gualandi, E. Scavettaa and D. Tonelli, *RSC Adv.*, 2016, **6**, 110976–110985.
8 Z. Z. Jiang, Z. B. Wang, Y. Y. Chu, D. M. Gu and G. P. Yin, *Energy Environ. Sci.*, 2011, **4**, 728–735.
9 H. S. Liu, C. J. Song, L. Zhang, J. J. Zhang, H. J. Wang and D. P. Wilkinson, *J. Power Sources*, 2006, **155**, 95–110.
10 S. Alayoglu, A. U. Nilekar, M. Mavrikakis and B. Eichhorn, *Nat. Mater.*, 2008, **7**, 333–338.
11 Z. L. Liu, X. Y. Ling, X. D. Su and J. Y. Lee, *J. Phys. Chem. B*, 2004, **108**, 8234–8240.
12 W. J. Zhou, S. Q. Song, W. Z. Li, Z. H. Zhou, G. Q. Sun, Q. Xin, S. Douvartzides and P. Tsiakaras, *J. Power Sources*, 2004, **140**, 50–58.
13 X. W. Zhou, R. H. Zhang, Z. Y. Zhou and S. G. Sun, *J. Power Sources*, 2011, **196**, 5844–5848.
14 J. M. Cao, J. Zhou, Y. F. Zhang, Y. X. Wang and X. W. Liu, *ACS Appl. Mater. Interfaces*, 2018, **10**, 1752–1760.
15 Y. Zhang, Y. W. Liu, M. Ma, X. Ren, Z. A. Liu, G. Du, A. M. Asiri and X. P. Sun, *Chem. Commun.*, 2017, **53**, 11048–11051.
16 C. Tang, L. S. Xie, K. Y. Wang, G. Du, A. M. Asiri, Y. L. Luo and X. P. Sun, *J. Mater. Chem. A*, 2016, **4**, 12407–12410.
17 C. Tang, R. Zhang, W. B. Lu, Z. Wang, D. N. Liu, S. Hao, G. Du, A. M. Asiri and X. P. Sun, *Angew. Chem., Int. Ed.*, 2017, **56**, 842–846.
18 X. L. Xiong, C. You, X. Q. Cao, L. F. Pang, R. M. Kong and X. P. Sun, *Electrochim. Acta*, 2017, **253**, 517–521.
19 W. J. Shi, Q. Wang, F. Qin, J. Yu, M. Jia, H. Gao, Y. Zhang, Y. Zhao and G. Li, *Electrochim. Acta*, 2017, **232**, 332–338.
20 J. Wang, Q. Zhao, H. Hou, Y. Wu, W. Yu, X. Ji and L. Shao, *RSC Adv.*, 2017, **7**, 14152–14158.
21 S. Li, W. Guo, B. Yuan, D. Zhang, Z. Feng and J. Du, *Sens. Actuators, B*, 2017, **240**, 398–407.
22 P. Wang, Y. Zhou, M. Hu and J. Chen, *Appl. Surf. Sci.*, 2017, **392**, 562–571.
23 J. F. Chang, L. G. Feng, C. P. Liu, W. Xing and X. L. Hu, *Angew. Chem., Int. Ed.*, 2014, **53**, 122–126.
24 G. Li, L. Feng, J. Chang, B. Wickman, H. Gronbeck, C. Liu and W. Xing, *ChemSusChem*, 2014, **7**, 3374–3381.
25 J. Chang, L. Feng, C. Liu, W. Xing and X. Hu, *Energy Environ. Sci.*, 2014, **7**, 1628–1632.
26 J. M. Cao, J. Zhou, Y. F. Zhang and X. W. Liu, *Sci. Rep.*, 2017, **18**, 8825.
27 J. Zhou, J. M. Cao, Y. Z. Zou, Y. F. Zhang and X. W. Liu, *Microelectron. Eng.*, 2017, **176**, 89–93.
28 J. M. Cao, X. L. Zhang, Y. F. Zhang, J. Zhou, Y. N. Chen and X. W. Liu, *PLoS One*, 2016, **11**, e0161374.
29 J. M. Cao, J. Zhou, Y. F. Zhang, Y. Z. Zou and X. W. Liu, *PLoS One*, 2017, **12**, e0177258.
30 C. H. An, Y. J. Wang, Y. P. Wang, G. Liu, L. Li, F. Y. Qiu, Y. A. Xu, L. F. Jiao and H. T. Yuan, *RSC Adv.*, 2013, **3**, 4628–4633.
31 H. Huang, H. Chen, D. Sun and X. Wang, *J. Power Sources*, 2012, **204**, 46–52.
32 G. M. Zhou, D. W. Wang, F. Li, L. L. Zhang, N. Li, Z. S. Wu, L. Wen, G. Q. Lu and H. M. Cheng, *Chem. Mater.*, 2010, **22**, 5306–5313.
33 Y. Huang, X. L. Huang, J. S. Lian, D. Xu, L. M. Wang and X. B. Zhang, *J. Mater. Chem.*, 2012, **22**, 2844–2847.
34 Y. Lu, X. L. Wang, Y. J. Mai, J. Y. Xiang, H. Zhang, L. Li, C. D. Gu, J. P. Tu and S. X. Mao, *J. Phys. Chem. C*, 2012, **116**, 22217–22225.
35 Q. F. Li, R. H. He, J. A. Gao, J. O. Jensen and N. J. Bjerrum, *J. Electrochem. Soc.*, 2003, **150**, A1599–A1605.
36 I. Esparbe, E. Brillas, F. Centellas, J. A. Garrido, R. M. Rodriguez, C. Arias and P. Cabot, *J. Power Sources*, 2009, **190**, 201–209.
37 Z. H. Zhang, Y. J. Huang, J. J. Ge, C. P. Liu and W. Xing, *Electrochem. Commun.*, 2008, **10**, 1113–1116.
38 Y. Chang, G. Han, M. Li and F. Gao, *Carbon*, 2011, **49**, 5158–5165.
39 Y. Y. Shao, S. Zhang, C. M. Wang, Z. M. Nie, J. Liu, Y. Wang and Y. H. Lin, *J. Power Sources*, 2010, **195**, 4600–4605.